High-pressure vibrational properties of dense rubidium

High Pressure Vibrational Properties of Dense Rubidium

Mario Santoro[1*], Daniele Colognesi[2], Bartomeu Monserrat[3], Eugene Gregoryanz[4], Lorenzo Ulivi[2], Federico A. Gorelli[1]

[1]*National Institute of Optics, INO-CNR, and LENS, via N. Carrara 1, I-50019 Sesto Fiorentino, Italy*

[2]*Institute of Applied Physics, IFAC-CNR, via Madonna del Piano 10, I-50019 Sesto Fiorentino, Italy*

[3]*TCM Group, Cavendish Laboratory, University of Cambridge, J. J. Thomson Avenue, Cambridge CB3 0HE, United Kingdom*

[4]*School of Physics and Astronomy, CSEC, Univ. of Edinburgh, Edinburgh EH9 3JZ, United Kingdom*

* Email: santoro@lens.unifi.it

Abstract. *At ambient conditions, alkali metals adopt the body centered cubic structure, while if compressed up to tens of GPa and above, they exhibit complex low symmetry modifications, due to the density-driven transition of the valence electrons from the s-state to states of higher angular momentum. These high-pressure, low-symmetry phases, whose unit cells may include up to tens of atoms, allow rich Raman activity, which was previously observed only in lighter alkalis Na and Li. Here we report an extensive study of the optical phonons of highly dense Rb up to 100 GPa in diamond anvil cells, conducted by challenging experimental Raman spectroscopy measurements and ab initio computer simulations. The relative (relative to the normal condition value) density behavior of Raman frequencies of Rb is compared to the one of Na and Li, once the frequencies of the two light alkali elements have been rescaled by* $\sqrt{M_{Na}/M_{Rb}}$ *and* $\sqrt{M_{Li}/M_{Rb}}$*, respectively, where* M_{Na}*,* M_{Li} *and*

M_{Rb} are the atomic masses of the here considered alkali elements. Importantly, while the rescaled density behaviors of Na and Li agree with each other, Rb significantly differs, which highlights the different nature of the valence electron transition being of the s-d and of the s-p type in heavy and light alkali metals, respectively, a result that calls for further similar investigations on K and Cs.

I. Introduction. At pressures above 10 GPa, alkali metals exhibit complex low-symmetry crystalline phases, whose existence is bound to the density-driven change of character of the valence electron from the *s*-type to states of higher angular momentum, namely *s-p* and *s-d* transition for light, Li and Na, and heavy, K, Rb and Cs, elements, respectively. Similarly, density- driven simple-to-complex phase transitions were also observed in the liquid state for Cs and Rb[1,2,3], due to the change of character of the valence electron. Interestingly, the high pressure, low symmetry crystalline phases of these systems allow a rich Raman activity, whose experimental observation has been so far limited to the light alkali metals[4,5,6]. Raman observations on these systems, combined with *ab initio* computer simulations, have been providing insight into the nature of microscopic interactions and, specifically, to the *s-p* transition, to the interaction between valence and core electrons at hundreds of GPa pressure, and to the quantum zero-point atomic motions for the particular case of Li[6]. Indeed, Raman experiments on the alkali metals, as on any other metal, are very challenging because of the small Raman cross section of the metallic state and to the very small scattering volume, whose thickness is limited to one optical wavelength or less. Nevertheless, these kinds of experiments are nowadays possible even in an additionally restrictive experimental environment such as that of the diamond anvil cell used for static high pressure investigations. Having successfully performed Raman spectroscopy measurements on light alkalis[5,6], we have decided to study the vibrational properties of a heavier alkali Rb, aiming to investigate the change of character of the valence electron by comparing to the light alkali metals. The structural properties of Rb under pressure, along with the phase diagram of this elemental system (figure 1), were extensively investigated both in the solid and the liquid state[7,8,9,10,11,12,13,14,15,16,17,18,19,2,20,3]. The knowledge of structural properties and equation of

state are necessary requirements for the quantitative interpretation of vibrational properties we aim to investigate.

At room temperature, solid Rb undergoes a pressure induced bcc (Rb I)-to-fcc (Rb II) phase transition, similarly to all other alkali metals, at 7 GPa (see [14] for review). This is a rather intuitive density driven phase transformation from a more open to a close compact structure. But if pressure is increased further, a sequence of somewhat counterintuitive phase transitions occurs at above 13 GPa to more open and less symmetric structures: Rb II-Rb III at 13.2 GPa, Rb III-IV at 16.5 GPa, Rb IV-Rb V at 20.2 GPa, and Rb V-Rb VI at 48 GPa[13,14,16,15,17,18], with Rb-VI experimentally found to be stable up to at least 1 Mbar[20]. Rb-III, also *oC*52, exhibits a very complex orthorhombic structure ($C222_1$) with 52 atoms per unit cell, a commensurate modulated stacking structure with an 8-10-8-8-10-8 stacking of 8- and 10-atom layers[16]. Rb-IV was originally identified as being a host-guest tetragonal structure (*I*4/*mcm*), made up of columns of face-sharing square antiprisms formed by one subset of Rb atoms (16 per unit cell) and quasi-one dimensional channels in between these columns (the host) occupied by a second subset of Rb atoms (the guest)[13]. Subsequently, the host-guest nature of Rb-IV was shown to be incommensurate[15], with the guest chains of atoms losing both the inter-chain and the intra-chain long range order upon pressure decrease below 16.7 GPa, thereby resulting in a sort of confined 1D liquid: "chain melting"[17]. Rb-V is a much simpler phase with a tetragonal structure ($I4_1/amd$, Z=4, tI4)[10], while Rb-VI has an orthorhombic symmetry (*Cmca*, *oC*16) with 16 atoms per unit cell[14]. Importantly, the driving force for this sequence of transitions is the density driven *s-d* electronic transition, which is now thought to be essentially completed at the pressure of the V-VI phase transition[14]. Above 48 GPa, solid Rb can be thought as a transition metal-like system, which is predicted to transform at above 143 GPa into a metallic close compact structure, namely a double-hexagonal-close-packed structure stable to at least 250 GPa[19].

Firstly, we will describe the experimental methodology, i. e. the sample preparation and Raman set-up, and the *ab initio* computer simulation methodology adopted in this study. In the subsequent sections, we will present and discuss the vibrational data obtained in four high-pressure Raman active

phases, namely Rb-III, -IV, -V and -VI, up to about 100 GPa, along with the comparison to literature vibrational data for the light alkalis. This comparison will underline some general effects of density driven changes of character (orbital angular momentum) of the valence electron in alkali metals.

II. Experimental and *ab initio* calculation methods and procedures. High purity Rb taken from an ingot of 99.6% purity (from Sigma Aldrich) was loaded in membrane or screw-driven diamond anvil cells (DACs), in glove boxes equipped with ancillary tools as microscope, light sources, and camera under ultrahigh quality atmosphere, oxygen and moisture free (less than 2 and 0.5 ppm, respectively). The DACs were equipped with Raman-selected flat 500 μm and beveled 55/300 μm culet size diamond anvils for pressures up to about 25 GPa and 85 GPa, respectively, and Re gasket. Although the 55/300 mm culet size anvils allow to achieve pressures as high as 200 GPa, we limited our Raman aimed study to below 100 GPa, where the phase diagram and the structural properties of solid Rb were already known from the literature and could serve as the basis for the DFT calculation of Raman frequencies. For experiments up to 25 GPa, a 150 μm diameter hole was drilled in the 50 μm thick gasket. This hole was filled by a transparent, soft polyethylene pellet as the pressure transmitting medium, which was in turn laser drilled to provide an 80 μm diameter sample chamber. A micron-size fluorescent $SrB_4O_7:Sm^{2+}$ chip was placed in the polyethylene as an optical pressure sensor[21,22]. Pressure shift of the Raman diamond edge was also used for measuring pressures[23], and the difference between the samarium borate and the diamond pressures was found to be 0.1 GPa or less, above 10 GPa. For experiments at higher pressures, up to 85 GPa, Rb was directly loaded in a 10 μm diameter hole drilled in the pre-indented gasket, similarly to all other literature investigations on solid Rb[7,8,9,10,11,12,13,14,15,16,17,18,20]. The use of inert noble gases to be cryo- or gas-loaded in the DAC as the pressure transmitting medium was prevented by the needs to confine the entire loading procedure within the highly purified glow box, since Rb is strongly hygroscopic. On the other hand, polyethylene and Rb itself are rather soft materials, which guarantees reliable

hydrostatic conditions in both our sample configurations. Sample quality in the different phases, at various pressures, was checked several times by measuring the X-ray diffraction pattern, and comparing it to literature data, by means of our in-house, custom X-ray diffractometer, equipped by a Mo source (Xenocs, GeniX Mo High Flux), with λ=0.7103 Å, and having a beam spot diameter on the sample and a divergence of 50-100 μm and 0.2°, respectively, and a Princeton Instruments PI SCX 4300 CCD as the detector.

Raman measurements on Rb were performed by using the red Kr^+ laser radiation (λ=647.1 nm) as the excitation source, in order to minimize the fluorescence background from diamonds. The perfect backscattering geometry was used through a long working distance (30 μm) Mitutoyo 20 X microscope objective, allowing a laser beam spot on the sample of 2-3 μm in diameter. A spatial filter on the collected optical pathway was used for reducing the effective depth of field of our microscope and, as a consequence, the spurious Raman and fluorescence signals of the diamond anvils. In particular, the efficient rejection of the residual broad diamond fluorescence background was mandatory for measuring the very weak Raman spectra of Rb with good signal to noise ratio. The collected Raman signal of Rb was finally detected by a triple-grating monochromator (trivista555, Acton-Roper), coupled to a liquid nitrogen cooled CCD detector (Princeton Instruments Spec-10:100BR), with the first two stages operating in subtractive mode. The typical spectral resolution was about 0.5 cm^{-1}. Anti-Stokes Raman spectra of Rb were also collected together with their Stokes counterparts at a few selected pressure values, in order to check that all observed peaks indeed originate from inelastic scattering, similarly to what we have done previously in Na[5] and Li[6]. The collected diamond Raman signal and $SrB_4O_7:Sm^{2+}$ fluorescence signal were detected by the same monochromator/CCD set-up, where only a single stage of the triple monochromator was used along with notch filters[5,6].

The experimental study was conducted at ambient temperature, except a high temperature (120 °C) annealing performed at about 50 GPa in order facilitate the V-to-VI phase transition, as indicated in ref. [14].

In order to help both with the rubidium EOS and the assignment of the observed Raman spectral features, a number of DFT calculations have been carried out on Rb III, IV, V, and VI in a wide range of density and external pressure. We have made use of the CASTEP code, which employs a plane-wave basis set for the valence electrons, with the atomic cores being incorporated via either ultrasoft or norm-conserving pseudopotentials. The structural information on the symmetry of the investigated Rb phases was obtained from Refs. [16,10,14] for Rb III, V, and VI, respectively, while for the incommensurate Rb IV phase we used an approximant structure of space group $P\text{-}42_1m$ and containing 58 atoms in the primitive cell. We note that a truly incommensurate structure has an infinitely large primitive cell, but approximants have been successfully used to describe these structures in the past. The code has been described in detail elsewhere[24]. However, it is worth mentioning one of the main features of the CASTEP code: the internal atom coordinates can be automatically relaxed so that the structure with the minimum total energy is obtained either by keeping the cell size fixed (constant volume minimization) or by imposing a selected value for the external pressure (constant pressure minimization). In the present study the latter approach has been chosen for Rb III, IV, V, and VI.

Dealing with the Rb pseudopotential our preference went to a reciprocal-space norm-conserving one generated for the ionized state and treating *4s* and *4p* orbitals as valence. A gradient-corrected form of the exchange-correlation functional, the *generalized gradient approximation* by *Perdew, Burke,* and *Ernzerhof* (GGA-PBE)[25], was employed for all the DFT simulations. Calculations were made using only one plane-wave cutoff value: E_{cut}=330 eV with a self-consistent field accuracy $\varepsilon=5.0\cdot10^{-7}$ eV/atom. This cutoff yielded well-converged properties of the fully relaxed structure with a Hellman-Feynman residual force lower than f=0.01 eV/Å and an energy precision $e=5.0\cdot10^{-6}$ eV/atom. The Brillouin zone sampling was performed using special k-points automatically generated

by the code with a grid separation of Δk=0.04 Å^{-1}, even though some test calculations with Δk=2π·0.03 Å^{-1} have been also done, showing negligible differences. The incommensurate Rb IV phase needs to be treated separately because the incommensurate nature manifests itself in the approximant structure as a small energy difference between different positions of the guest chain relative to the host structure. To be able to properly capture the energetics of the approximant structure, we therefore used a finer plane-wave cutoff value of E_{cut}=700 eV with a self-consistent field accuracy of ε=1.0·10^{-10} eV/atom and Hellman-Feynman residual forces lower than f=0.0001 eV/Å. The Brillouin zone was also sampled with a finer grid separation of Δk=2π·0.025 Å^{-1}.

Once the final fully relaxed structures (still complying with the respective symmetry constraints) were obtained providing the requested cell volumes, phonons at the Γ point were evaluated through an internal CASTEP routine, pointing out the Raman and infrared frequencies of optically active modes. Special care was devoted to check that no imaginary frequencies were obtained (with the possible exception of the three immaterial acoustic modes). The phonon calculations for the incommensurate structure were treated separately using an in-house code that implements the finite displacement method[26].

III. Results and discussion. In figure 2, we report a selection of representative, experimental Raman spectra of solid Rb, together with empirical peak fits: Rb-III at 14.8 GPa, Rb-IV at 16.9 GPa, Rb-V at 21.7 GPa and Rb-VI at 63.5 GPa, measured upon increasing (IV, V, and VI) and decreasing (III) pressure. The collection time amounted to 30 min for Rb-IV and Rb-VI and to 60 min for Rb III and Rb V. A spurious, straight-light, smoothly frequency-dependent background has been subtracted from all the spectra. This background amounts to at most 20 percent of the total scattered intensity at frequencies as low as 25-30 cm^{-1} and monotonically decreases upon increasing the Raman shift. The four spectra have been then vertically normalized for the same peak intensity, and shifted for the sake of clarity. No Raman peaks were detected above 400 cm^{-1} at any pressure, and no Raman signal was detected below 13 GPa, according with Rb being Raman inactive in the two phases stable below this

pressure: Rb-I, bcc, and Rb-II, fcc. Interestingly, the signal to noise, S/N, ratio, is at a maximum for the spectrum of Rb-V, which could be due to this phase exhibiting a reduced reflectivity and, consequently, an increased scattering volume with respect to the other phases. Indeed, optical data in the visible spectral range, unfortunately limited to 1.1 GPa, indicate that the reflectivity of Rb decreases upon increasing pressure[7]. Other optical data extended up to 25 GPa, but limited to the near IR spectral region, show that the reflectivity of Rb decreases upon increasing pressure with a minimum corresponding to the pressure range of Rb-IV, whereas Rb-V has a slightly higher reflectivity[8]. Of course, pressure behavior of the Raman cross section, which is unknown, is also expected to affect the pressure dependence of the S/N ratio. A close glance to the experimental spectra and Raman DFT frequencies (also reported in figure 2 as vertical ticks) provides a rich description of the Brillouin zone center, vibrational dynamics of solid rubidium in the four different crystalline phases. The measured Raman spectrum of Rb III at 14.8 GPa ranges from 20 cm^{-1} to 150 cm^{-1}, and it includes at least 8 well resolved or almost resolved distinct peaks with significantly different full width at half maximum, FWHM, of 4-6 cm^{-1} (3 peaks) and 15-22 cm^{-1} (5 peaks) at the most. This phase has 26 atoms in the primitive cell, which implies an extremely rich vibrational pattern made of 75 expected optical modes, all Raman active, with symmetry: $19B_1+18B_2+19B_2+19A$. DFT simulations for this phase report indeed 75 distinct frequencies with inter-spacing as small as tenths of a wavenumber, over a range which compares quantitatively to the frequency range of the experimental Raman spectrum. Of course, the large density/defect induced broadness of the observed peaks, as compared to the inter-spacing of DFT frequencies, severely limits the assignment of these peaks to single expected optical modes. The measured Raman spectrum of Rb IV is a little bit simpler than that of Rb III, as it includes only 5 rather broad (FWHM of 15-25 cm^{-1}), well resolved peaks, spaced each other by 20-35 cm^{-1}, lying in the frequency range of 20-180 cm^{-1} at 16.9 GPa. As described earlier, we simulated Rb IV using a commensurate approximant host-guest structure of space group $P\text{-}42_1m$ and 58 atoms in the primitive cell, which leads to a total of 171 optical phonon modes at each wave vector. For this structure, 153 modes are Raman active with symmetries

$45E+22B_2+23A_1+18B_1$. Our DFT calculated frequencies at 18.0 GPa cover the range 1-169 cm^{-1}, which, similarly to phase III, compares quantitatively to the frequency range of the experimental Raman spectrum above 20 cm^{-1}. Interestingly, a Raman active phason mode with a frequency of 1.3 cm^{-1} at the Γ-point is predicted to span the full Brillouin zone plane perpendicular to the incommensurate axis. Phason modes, which correspond to the sliding of the guest chain relative to the host structure, are well-known to arise in incommensurate structures, and can lead to exotic properties such as strong coupling superconductivity[27]. Although in our approximant simulation cell this mode has a finite frequency, the larger the approximant cell the lower the frequency of the phason mode will become, and it should tend to zero in the infinite cell limit, which corresponds to the approximant structure converging to the real incommensurate structure. The Raman spectrum of Rb V shows only two intense peaks, at around 55 cm^{-1}, FWHM ≈ 4 cm^{-1}, and 162 cm^{-1}, FWHM ≈ 13 cm^{-1}, respectively, at 21.7 GPa. These two peaks are exactly what is expected for this relatively simple structure, which has 2 atoms in the primitive cell and hence 3 optical modes, all Raman active: E_g+B_{2g}. Indeed, since E_g is doubly degenerate, only two distinct Raman peaks are expected. The comparison of experimental and DFT frequencies is very good, and we can straightforwardly assign the low and high frequency observed peaks to the E_g and B_{2g} modes, respectively. Finally, Rb VI exhibits up to 7 distinct experimental Raman peaks, FWHM of 15-30 cm^{-1}, not all of which are visible at all pressure values, in the frequency range of 80-400 cm^{-1}. In figure 2, we report the spectrum of Rb VI measured at 63.5 GPa. Rb VI again is a rather complex phase with 8 atoms per primitive cell and 12 Raman active modes, with symmetry: $2B_{1g}+3B_{2g}+3B_{3g}+4A_g$. The overall agreement between the experimental spectrum and the 12 distinct DFT frequencies is rather good.

In figure 3 we report the pressure shift of all experimentally observed and DFT calculated Raman frequencies from about 13 GPa to 100 GPa. The experimental frequencies were obtained by fitting the Raman spectra to a sum of Gaussian peak functions, with the sole exception of the high frequency B_{2g} peak of Rb V, which was instead fit to an asymmetric peak function. This asymmetry may be ascribed to the Fano resonance of the involved optical phonon with the continuum energy

spectrum of conduction electrons, an already well known effect in heavily doped semiconductors and poor metals[28,29,30]. Pressure ranges of frequencies ascribed to different phases agree well with the phase diagram of solid Rb. Some metastable extensions beyond phase boundaries are also observed, through the characteristic Raman frequencies, such as that of Rb IV into V and Rb V into VI and vice versa. Remarkably, the overall spread of frequencies significantly increases upon pressure increase, from about 120 cm^{-1} at 14 GPa to about 260 cm^{-1} at 100 GPa, and the average frequency also increases by almost a factor of 3 over this pressure range, which immediately signals a strong increase of the interatomic interaction. Also noticeable, the overall agreement between observed and DFT frequencies is rather good at all pressures, which in turn validates the DFT predictions and reasonably allows to extend their validity to other observables such as the lattice parameters and the equation of state, EOS.

We can now use our vibrational data for providing a somewhat general view on dynamical properties of alkali metals, by comparing these data to vibrational data of Na and Li available in the literature[4,5,6]. In order to proceed in this analysis, we need to consider that the meaningful independent variable is the reduced density (density normalized to the value at ambient pressure) rather than pressure. We thereby need to consider the EOS of Rb, along with those of Na and Li[31]. In figure 4, we show these EOSs in terms of relative atomic volume vs. pressure. Here, the attention is focused on the high pressure Raman active phases, which occur at pressures above 13 GPa, 35 GPa and 108 GPa for Rb, Li and Na, respectively. For Rb, our DFT EOS compares very well to the experimental EOS[16,13,14] for all phases, which in turn is limited to about 50 GPa. DFT results then extend the EOS of Rb up to about 100 GPa, which is a factor of 2 in pressure. One striking aspect should now attract the main attention when comparing EOSs for light and heavy alkali metals. It is clear that Na and Li are rather similarly compressed in the common range of pressures, with Na being slightly softer and the relative volume of Na and Li amounting to 0.26-0.21 at 108-160 GPa, whereas Rb is much more compressible with a relative volume of 0.26 at 24 GPa and as small as 0.15 at 100 GPa. It is straightforward to ascribe the similar compression of light alkali metals to the valence electron for

these elements undergoing the *s-p* transition, whereas the corresponding *s-d* transition for the heavier Rb makes this metal much more compressible. This argument implies that the interatomic chemical bonds supported by *d*-type valence electrons are more flexible that those supported by *p*-type valence electrons. One may then wonder if optical mode frequencies of the alkali metals, when properly rescaled for the different masses and considered as functions of relative compression, would exhibit a common relationship.

In figure 5, we report the observed and calculated Raman frequencies of Rb, as in figure 4, this time plotted as a function of the reduced density. The range of ρ/ρ_0 extends from about 2.9 to about 6.5, and the density behavior of frequencies appears to be essentially linear. In the same figure, we also report the behavior of selected Raman frequencies for Li[6] and Na[4,5], mass rescaled as $\nu_{rLi(Na)} = \nu_{Li(Na)}\sqrt{M_{Li(Na)}/M_{Rb}}$, where $\nu_{rLi(Na)}$ and $\nu_{Li(Na)}$ are the rescaled and not rescaled frequency of Li (Na), respectively, and M_{Li}, M_{Na} and M_{Rb} are the atomic masses of the considered alkali elements. The selected Raman frequencies for Li and Na, whose high pressure phases also exhibit a very rich Raman spectrum at reduced densities above 2.4 (Li) and 3.8 (Na), are the highest and the lowest Raman frequency at each pressure, respectively. Thereby, these two frequencies provides a rough estimate of the whole extension of the vibrational density of state, v-DOS, for compressed Li and Na. Indeed, we aim to base the comparison between the three different elemental systems on this key observable, namely the frequency range of v-DOS. Remarkably, the whole extensions of mass rescaled v-DOS of Li and Na agree fairly well with each other in the common density range, which, as a consequence, constitutes a master relationship for light alkali metals. On the other hand, both behaviors for the total frequency range substantially differ from that of Rb. For instance, the mass-rescaled frequency range of the two light elements is larger than that of Rb by a factor of about 1.9 at ρ/ρ_0=2.9 and 1.4 at ρ/ρ_0=4.9, hence phonons of Rb are also softer. The similar behavior of Li and Na and the difference between these two elements and Rb can be easily attributed to both the light alkali metals undergoing the *s-p* transition, as opposite to the heavy alkali elements

instead undergoing the *s-d* transition. It is then not possible to build up a general master graph including the frequencies of all alkali metals, but instead light and heavy ones must be considered separately, due to the very different density behavior of the valence electron. Interestingly, at reduced density of about 5, Na undergoes the striking metal-to-insulator phase transition via *p-d* hybridization of the valence electrons, although the *p* character still dominates, and their repulsion by core electrons into the lattice interstices[4,5]. Correspondingly, the frequency range of optical phonons of Na decreases by a factor of about 1.3, as it can be deduced from reference[4].

The Grüneisen parameters, γ_i, for the Raman active optical modes of Rb can now be calculated from the density dependence of the frequencies ν_i, reported in figure 5, as: $\gamma_i = \rho^*/\nu_i \cdot \partial\nu_i/\partial\rho^*$, where *i* labels the mode, and ρ^* is the reduced density. The Grüneisen parameters, γ_i, of the two modes of phase V differ by less than 5 % and decrease from about 1.61/1.65 to 1.34/1.38 upon increasing density over the entire stability range of this phase. On the other hand, γ exhibits substantially different values among all the modes of Rb VI, ranging from 0.71 to 1.44 as the maximum and minimum values at all densities. In the inset of figure 5, we report the average values of γ for Rb V and Rb VI as a function of density. Interestingly, the average value of γ decreases upon increasing density in Rb V, whereas it is rather constant in Rb VI, with a significant drop at the phase transition. This change can be reasonably understood as arising from the end of the *s-d* transition at the V-to-VI phase transition. An indirect and rough estimate of the average γ for Rb VI, obtained from previous synchrotron X-ray absorption measurements, is also reported in the inset (dot with error bar)[20]. The error bar indicates a range of possible values for the estimated γ. This range is not far from the present value for the average γ, although the agreement between results from these two methods is not very quantitative.

IV. Conclusions. We have investigated the optical modes of dense, compressed Rb, in its known low-symmetry Raman-active crystalline phases from 13 GPa to about 100 GPa, aiming to extend the knowledge of the optical response of heavier alkali metals and compare this with the lighter

alkalis such as Li[6] and Na[4,5]. We have plotted the master graph of dynamical properties of three alkali elements, with our combined experimental and calculated Raman data showing that, while dynamical properties of light alkali metals match a single unified density behavior, they substantially differ from those of Rb. This kind of comparison is the result of the different nature of the changes of the valence electrons, namely *s-p* and *s-d* transition for light and heavy elements, respectively. Similar investigations on K and Cs can further extend and confirm this view. It is feasible that the dynamical properties of light and heavy alkali elements may follow two separate, master density behaviors.

V. Acknowledge. We acknowledges the PRIN project ZAPPING, No. 2015HK93L7, granted by the Italian Ministry of Education, Universities and Research, MIUR, supporting our research in high pressure materials science. B. M. acknowledges support from the Winton Programme for the Physics of Sustainability, and from Robinson College, Cambridge, and the Cambridge Philosophical Society for a Henslow Research Fellowship.

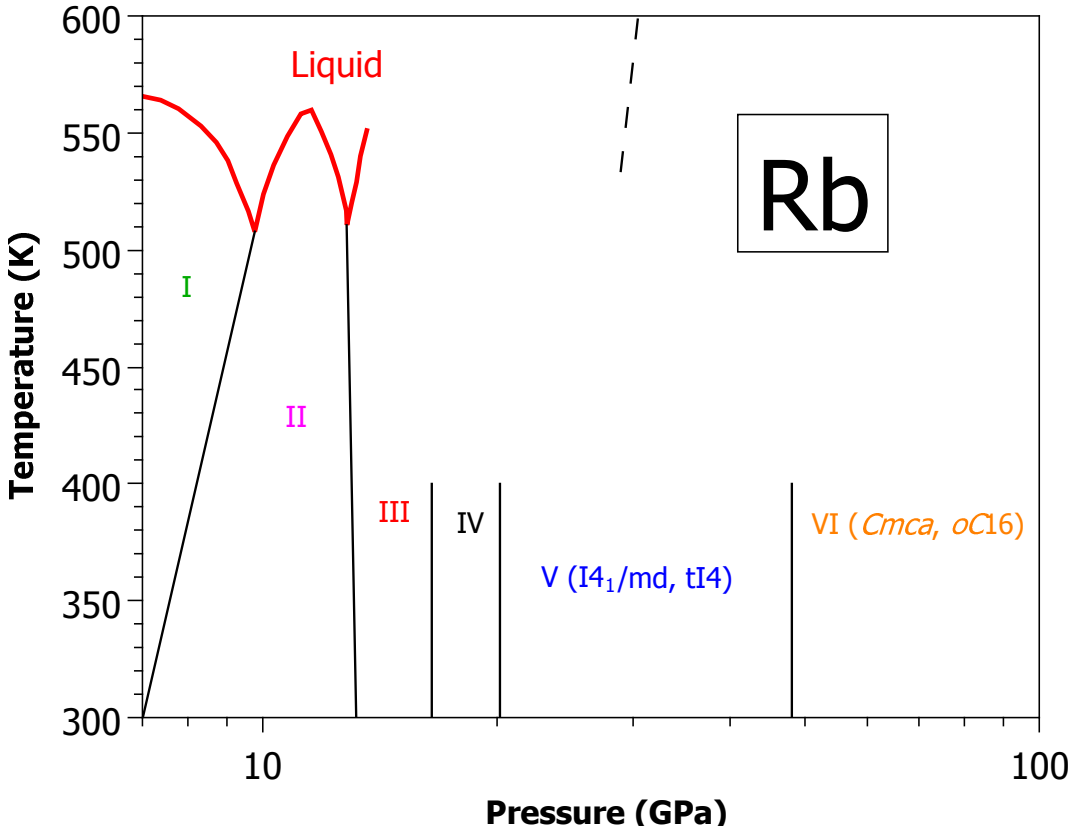

Figure 1. (Color on line) High-pressure phase diagram of Rb[13,14,16,15,17,18,20,3]. The dashed line is a hypothetical phase boundary passing through the only single melting point observed along an isotherm decompression at 573 K. The high temperature extensions of the solid-solid phase transitions are also hypothetical, as these phase transitions have only been investigated at room temperature.

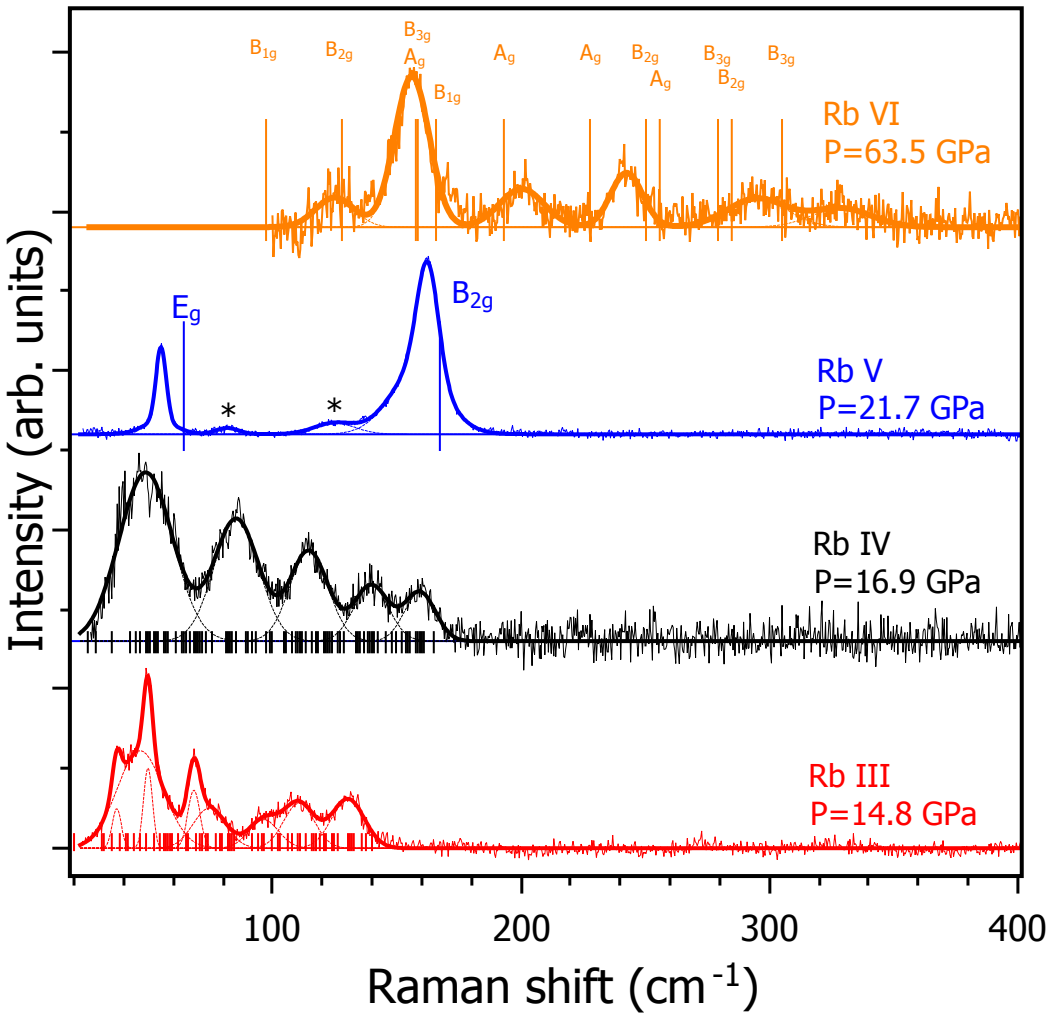

Figure 2. (Color on line) Representative Raman spectra of dense Rb in phases III, IV, V and VI. Continuous, thin lines: measured spectra. Dashed and continuous thick lines: single Gaussian peak and total fit to experimental data, respectively. Vertical ticks: DFT frequency values (DFT frequencies for Rb IV have been calculated at 18.0 GPa). Mode symmetry for the DFT frequencies of phase V and VI are also reported. Stars: peaks assigned to phase IV metastable in the stability pressure domain of phase V.

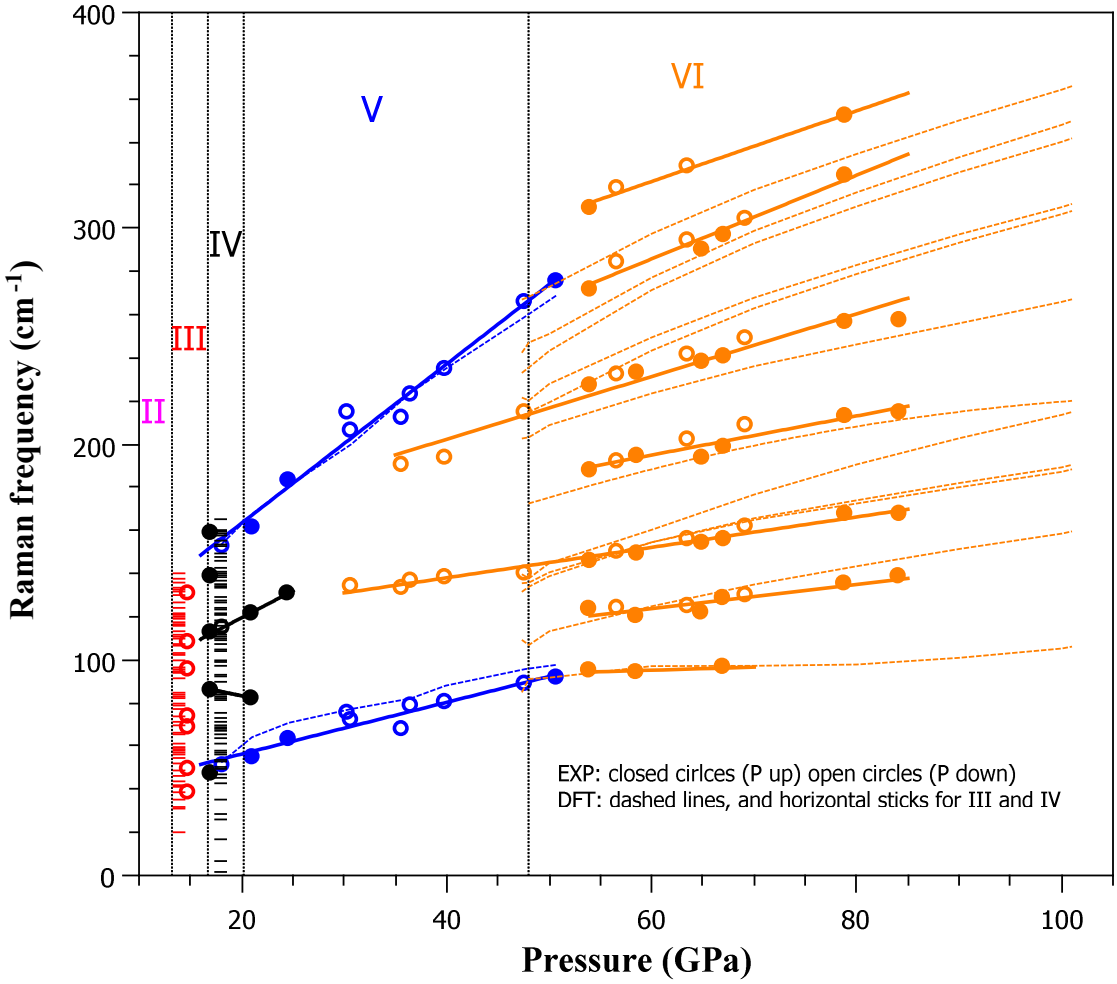

Figure 3. (Color on line) Pressure shift of measured and DFT calculated Raman frequencies in dense Rb. Different colors correspond to different phases, as in all other figures. Full and empty circles: experimental values measured upon increasing and decreasing pressure, respectively. Dashed lines: DFT values for Rb V and VI. Horizontal sticks: DFT values for Rb III and IV. Continuous lines: linear fit to the experimental points, as the guide to an eye. Vertical lines: phase boundaries between Rb II, III, IV, V and VI.

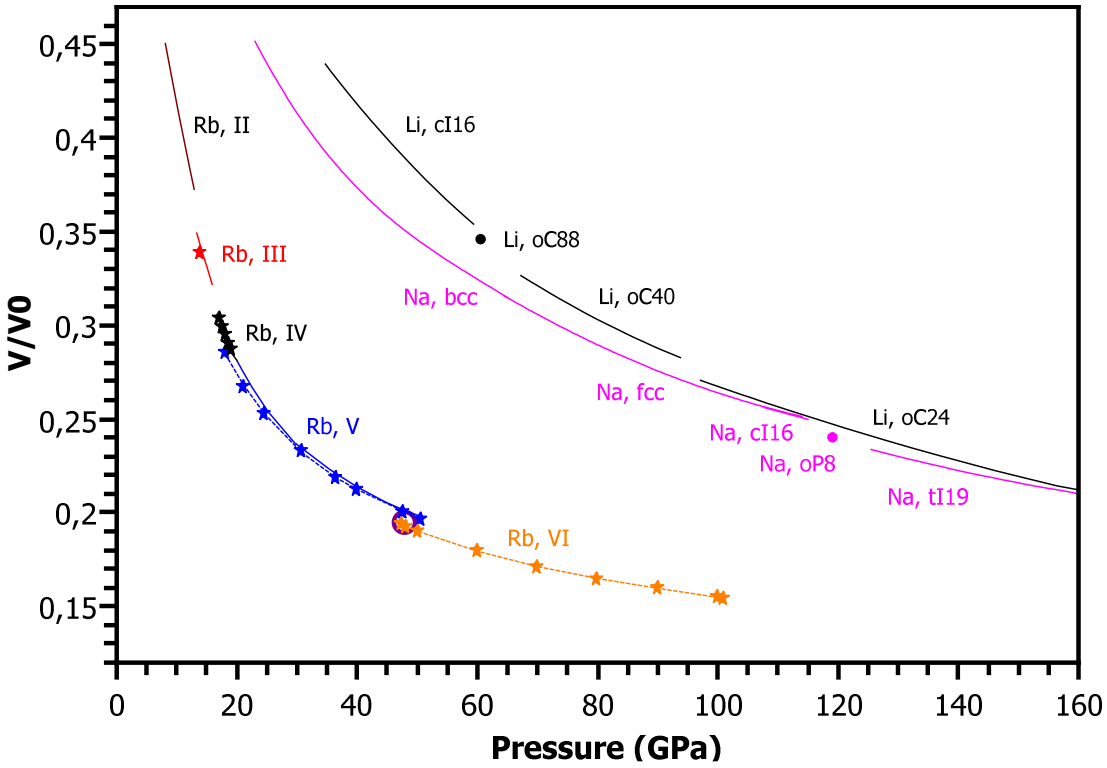

Figure 4. (Color on line) Equation of state of Rb. Stars and continuous colored lines: our DFT calculations and experimental data from literature[16,13,14], respectively. Li and Na equations of state are also reported from ref. [31]. Colors for Rb correspond to different phases as in all other figures. The purple open circle at around 48 GPa correponds to the only literature volume data for Rb VI[14]. The atomic volume V_0 is equal to 92.82 Å^3, 39.35 Å^3 and 21.75 Å^3 for Rb, Na and Li, respectively.

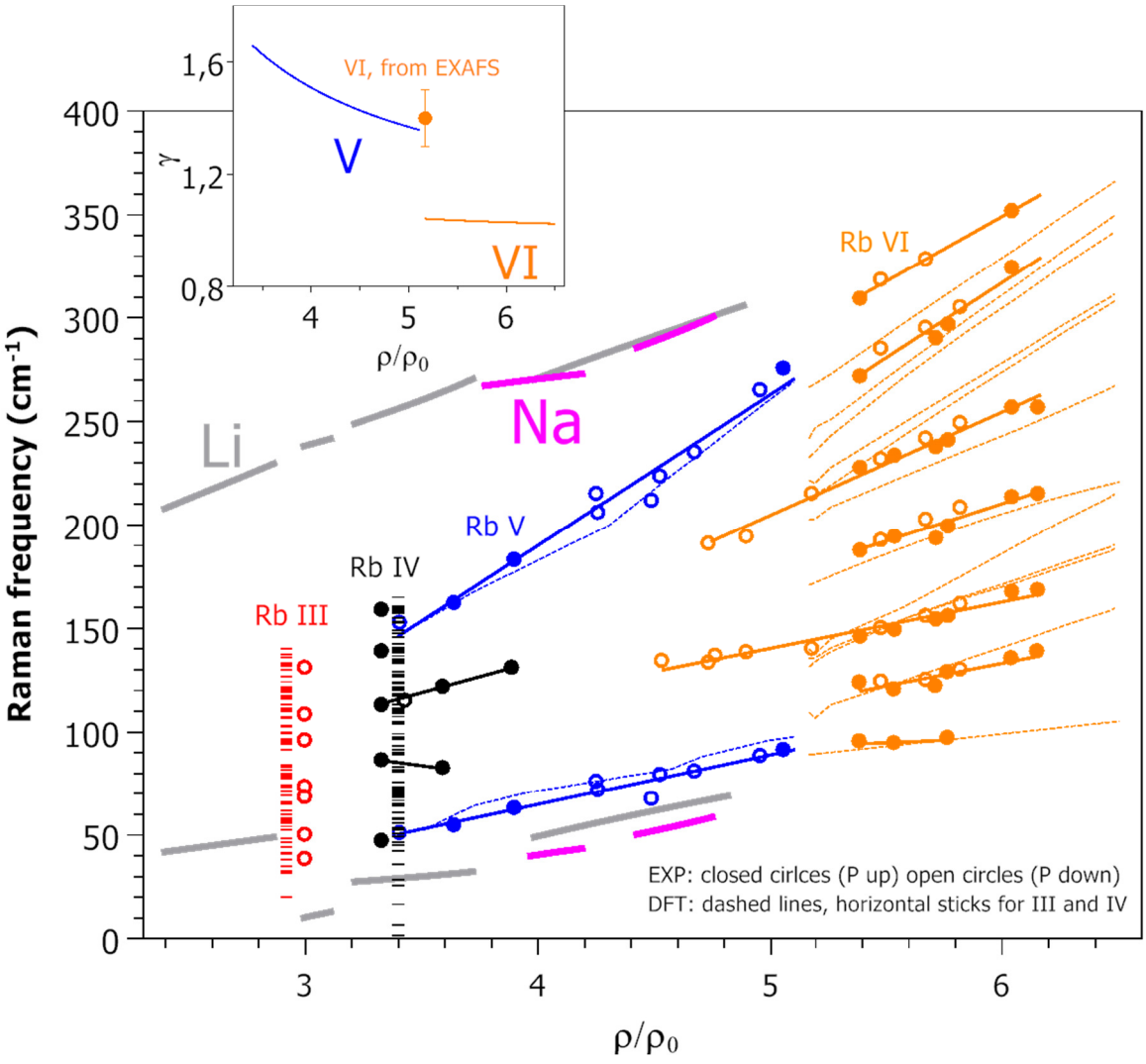

Figure 5. (Color on line) Measured and calculated Raman frequencies in dense Rb as a function of reduced density. Different colors correspond to different phases, as shown in all other figures. Full and empty circles: experimental values measured upon increasing and decreasing pressure, respectively. Dashed lines: DFT values for Rb V and VI. Horizontal sticks: DFT values for Rb III and IV. Continuous lines: linear fit to the experimental points, as the guide to an eye. Thick grey and magenta lines: relative density behavior of the highest and lowest, normalized to the Rb mass (see text) Raman frequencies for Li[6] and Na[4,5], respectively; different segments correspond to different phases. Inset, continuous lines: experimental average Grüneisen parameter vs. relative density for Rb V and Rb VI. Inset, dot with error bars: value of the Grüneisen parameter estimated in a previous XAS experiment[20].

References

[1]S. Falconi, L. F. Lundegaard, C. Hejny, M. I. McMahon, *Phys. Rev. Lett*. **94**, 125507 (2005).

[2]T. Bryk, S. De Panfilis, F. A. Gorelli, E. Gregoryanz, M. Krisch, G. Ruocco, M. Santoro, T. Scopigno, and A. P. Seitsonen, *Phys. Rev. Lett*. **111**, 077801 (2013).

[3]F. A. Gorelli, M. Santoro, S. De Panfilis, T. Bryk, L. Ulivi, G. Garbarino, and P. Parisiades, *J. Chem. Phys. Lett*. **9**, 2909 (2018).

[4]Y. Ma, M. Eremets, A. R. Oganov, Y. Xie, I. Trojan, S. Medvedev, A. O. Lyakhov, M. Valle, and V. Prakapenka, *Nature* **458**, 182 (2009).

[5]M. Marques, M. Santoro, C. L. Guillaume, F. Gorelli, J. Contreras-Garcia, R. T. Howie, A. F. Goncharov, and E. Gregoryanz, *Phys. Rev. B* **83**, 184106 (2011).

[6]F. A. Gorelli, S. F. Elatresh, C. L. Guillaume, M. Marques, G. J. Ackland, M. Santoro, S. A. Bonev, and E. Gregoryanz, *Phys. Rev. Lett*. **108**, 055501 (2012).

[7]K. Takemura, and K. Syassen, *Solid State Commun*. **44**, 1161 (1982).

[8]H. Tups, K. Takemura, and K. Syassen, *Phys. Rev. Lett*. **49**, 1776 (1982).

[9]M. S. Anderson and C. A. Swenson, *Phys. Rev. B* **28**, 5395 (1983).

[10]H. Olijnyk, and W. B. Holzapfel, *Physics Letters* **99A**, 381 (1983).

[11]R. Boehler, and M. Ross, *Phys. Rev*. B **29**, 3673 (1984).

[12]M. Winzenick, U. Vijayakumar, W. B. Holzapfel, *Phys. Rev. B* **50**, 12381 (1994).

[13]U. Schwarz, A. Grzechnik, K. Syassen, I. Loa, and M. Hanfland, *Phys. Rev. Lett*. **83**, 4085 (1999).

[14]U. Schwarz, K. Syassen, A. Grzechnik, M. Hanfland, *Solid State Commun.* **112**, 319 (1999).

[15]M. I. McMahon, S. Rekhi, and R. J. Nelmes, *Phys. Rev. Lett*. **85**, 055501 (2001).

[16]R. J. Nelmes, M. I. McMahon, J. S. Loveday, and S. Rekhi, *Phys. Rev. Lett*. **88**, 155503 (2002).

[17]M. I. McMahon, and R. J. Nelmes, *Phys. Rev. Lett*. **93**, 055501 (2004).

[18]M. I. McMahon and R. J. Nelmes, *Chem. Soc. Rev*. **35**, 943 (2006).

[19]Y. Ma, A. R. Oganov, and Yu Xie, *Phys. Rev. B* **78**, 014102 (2008).

[20]S. De Panfilis, F. Gorelli, M. Santoro, L. Ulivi, E. Gregoryanz, T. Irifune, T. Shinmei, I. Kantor, O. Mathon, and S. Pascarelli, *J. Chem. Phys*. **142**, 214503 (2015).

[21]J. Leger, C. Chateau, and A. Lacam, *J. Appl. Phys*. **68**, 2351 (1990).

[22]F. Datchi, R. LeToullec, and P. Loubeyre, *J. Appl. Phys*. **81**, 3333 (1997).

[23]Y. Akahama, and H. Kawamura, *J. Appl. Phys*. **100**, 043516 (2006).

[24]S. J. Clark, M. D. Segall, C. J. Pickard, P. J. Hasnip, V. Probert, K. Refson, M. C. Payne, *Z. Kristallogr.* **220**, 567 (2005).

[25]J. P. Perdew, K. Burke, M. Ernzerhof, *Phys. Rev. Lett.* **77**, 3865 (1996).

[26] J. H. Lloyd-Williams, and B. Monserrat, *Phys. Rev. B* **92**, 184301 (2015).

[27] P. Brown, K. Semeniuk, D. Wang, B. Monserrat, C. J. Pickard, and F. Malte Grosche, *Science Advances* **4**, eaao4793 (2018), DOI: 10.1126/sciadv.aao4793.

[28]F. Cerdeira, T. A. Fjeldly, and M. Cardona, *Phys. Rev. B* **8**, 4734 (1973).

[29]D. Olego and M. Cardona, *Phys. Rev. B* **23**, 6592 (1981).

[30]Y. Wang, S.-Q. Jiang, A. F. Goncharov, F. A. Gorelli, X.-J. Chen, D. Plăsienka, R. Martŏnák, E. Tosatti, and M. Santoro, *J. Chem. Phys*. **148**, 014503 (2018).

[31]C. L. Guillaume, E. Gregoryanz, O. Degtyareva, M. I. McMahon, M. Hanfland, S. Evans, M. Guthrie, S. V. Sinogeikin, and H-K. Mao, *Nature Physics* **7**, 211 (2011).